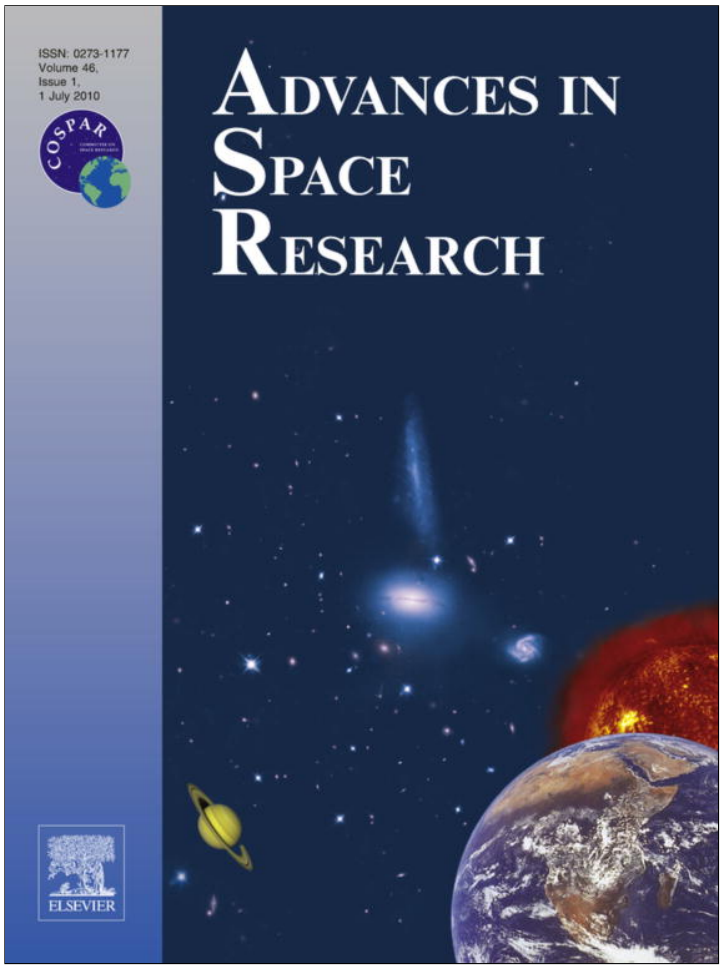

Available online at www.sciencedirect.com
ScienceDirect
Advances in Space Research 46 (2010) 22–30
ADVANCES IN SPACE RESEARCH (a COSPAR publication)
www.elsevier.com/locate/asr

A morphological study of CMEs using wavelet analysis ☆

D.I. González-Gómez [a,*], X. Blanco-Cano [a], A.C. Raga [b]

[a] Instituto de Geofisica, Universidad Nacional Autonoma de Mexico, Ciudad Universitaria, Mexico
[b] Instituto de Ciencias Nucleares, UNAM, Apartado Postal 70-543, 04510 México, DF, Mexico

Received 20 August 2009; received in revised form 6 February 2010; accepted 10 February 2010

Abstract

The principal objective of this study is to analyze structures of Coronal Mass Ejections (CMEs) using a wavelet technique. We use data measured with the SOHO/LASCO coronographs C2–C3, EIT and STEREO COR1A–B, COR2A–B. We have found that different structures show up in a CME at different spatial scales of wavelets. We also study the orientation of the most intense flux and find the orientation of the structures in the CME.

Keywords: CME – three parts structure; Wavelet analysis

1. Introduction

Coronal mass ejections (CMEs) are large eruptions of plasma and magnetic field from the Sun. Although only discovered in the early 1970s (Tousey, 1971; MacQueen et al., 1974), the effects of CMEs have been seen indirectly at Earth for thousands of years. Since their discovery, several thousand CMEs have been observed (Howard et al., 1985; Kahler, 1992; Webb et al., 1992; Hundhausen, 1997; Gosling, 1997; Bemporat et al., 2007) with a wide variety of instruments. White-light coronographs in space provide the bulk of the observations. The earlier observations from the OSO-7, Skylab, Solar Maximum Mission (SMM), and Solwind coronagraphs have been reviewed and compared with the current coronagraph observations from the Large Angle and Spectrometric Coronographs (LASCO) on Solar and Heliospheric Observatory (SOHO) by Gopalswamy et al. (2003). Yashiro et al. (2004) emphasized the LASCO CME annual variations, and Gopalswamy et al. (2004) empasized the mission – cumulative statistics.

Material ejections are a common phenomenon of the solar corona. Nevertheless, the mechanisms that cause a CME and the forces acting on it during its subsequent propagation through the corona are largely unknown. CMEs are massive (10^{14}–10^{17} g) clouds of plasma that are ejected from the Sun. One of the scientific objectives of LASCO is to understand why these events occur.

The LASCO (coronograph spacecraft) onboard the SOHO (Fleck et al., 1995 and Brueckner et al., 1995), launched in December 1995, provides to date unprecedented coronal images, due to its high cadence and spatial resolution of the Sun's corona. For the first time the Sun was observed continuously by SOHO, thanks to its vantage point in L1. At present two simultaneous corona images are also provided by STEREO (Solar Terrestrial Relations Observatory). This mission employs two nearly identical space-based observatories – one ahead of Earth in its orbit, the other trailing behind – to provide the first-ever stereoscopic measurements to study the Sun and the three-dimensional structure, this is the main target of the STEREO mission.

A few previous papers have used wavelet analysis techniques to study solar phenomena. (Stenborg et al., 2008) develop a technique to enhance EUV features based on

☆ This template can be used for all publications in Advances in Space Research.

* Corresponding author.
E-mail addresses: dulce@geofisica.unam.mx (D.I. González-Gómez), xbc@geofisica.unam.mx (X. Blanco-Cano), raga@nucleares.unam.mx (A.C. Raga).

0273-1177/$36.00 © 2010 COSPAR. Published by Elsevier Ltd. All rights reserved.
doi:10.1016/j.asr.2010.02.022

their multiscale nature. Using EIT data they showed the existence of some features that are not revealed with standard image-processing techniques, Stenborg and Cobelli (2003) used the wavelet analysis for the reduction of local noise and interactive weighted recomposition, they used data from LASCO-C1, C2 and C3. This approach represents a major advance towards unambiguous image interpretation and provides a means for the quantification of stationary and dynamic coronal structures required for morphological studies. Recently, Byrne et al. (2009) applied multiscale methods to enhance the visibility of the faint CME fronts. This enables an ellipse characterisation to study the changing morphology (width, orientation) and the kinematics (height, velocity, acceleration) of a sample of events imaged by LASCO and STEREO.

SOHO white-light images show that CMEs can have a variety of structures accordingly they can be clasified as: (1) Halo CME, (2) Helix CME and (3) Jets CME (Kahler, 2006; Gopalswamy et al., 2004; Cremades and Bothmer, 2004). The observed variety of structures is most likely due to the integration along the line of sight and to projection effects. The origin of a CME and its complex morphology are still not well understood.

The principal objective of this work is to analyze the morphological structures of a CME seen from different angles with different instruments, using the wavelet analysis technique. In Section 2, we describe the wavelet analysis technique used in this study. The observations details are given in Section 3. In Section 4 we give the results. In Section 5, we describe the orientation of the most intense flux that is present in a CME. Discussion and conclusions are given in Section 6.

2. Wavelet analysis

The main objective of this work is to use a wavelet analysis technique to study structures inside of CMEs at different spatial scales. The wavelet transform is essentially a convolution of one function with a set of base functions. As the base function we use the Mexican hat defined as

$$g(r) = C(2 - r^2)e^{r^{-2}/2}, \tag{1}$$

where $r = [x^2 + y^2]^{1/2}/a$, $C = (2a^2)^{-1/2}$, and a is the scale length of the wavelet. C is a normalization constant. The transform is obtained using the following: define a system of coordinates with y axis along the length, and x along the width of the box. The convolution is performed for the entire box (in this case the entire image) using the equation:

$$T_a(x,y) = \int\int I(x',y')g_a(r')dx'\,dy', \tag{2}$$

where $I(x,y)$ is the observed map, and $g(r')$ is the isotropic Mexican hat, with $r' = \sqrt{(x-x')^2 + (y-y')^2}/a$. These convolutions are calculated using a standard FFT algorithm.

The Mexican hat functions have null integrals $(\int\int g_a(r')dx'\,dy')$ for all values of a. Therefore, if a region of the image has intensity variations over scales $a_{Im} \gg a$, the transform will satisfy the condition $T_a(x,y) \approx 0$. Analogously, if the intensity variations have scales $a_{Im} \ll a$, the transform will also have very low values. Therefore, the $T_a(x,y)$ has large (positive or negative) values only in the regions of the image with intensity variabilities over spatial scales $a_{Im} \sim a$.

In this way, we can then choose a set of different values for the scale a of the wavelet, and compute the corresponding transforms (Eq. (2)) of the image. These transforms are representations of the image which only show the structures which have spatial scales similar to the scale a of the wavelet that has been used.

3. Observations

Fig. 1 shows a CME event observed by SOHO/LASCO (C2 and C3 cameras), EIT and STEREO (COR1, COR2 cameras, which are separated in space by an angle of 44°). The date of the event January 2, 2008. The event has been classified in the catalogue of LASCO as Partial Halo . The white-light image of this CME shows the typical three-part structure that was first described by Illing and Hundhausen (1983) (see Fig. 1A and D).

The pixel sizes of the C2 and C3 coronagraphs of LASCO are 11.4 and 56 arcsec, respectively, and the fields of view (FOV) range from 1.5 to 6 $R_\odot$ for C2, and 3.7 to 30 $R_\odot$ for C3, while the typical time resolution is around 12 min, to full resolution images of 1024 × 1024 pixels in FITS format. An important fraction of CMEs show a three-part structure consisting of a frontal structure (bright leading edge), a cavity (dark void), and a core (bright core) (Hundhausen, 1999; Gopalswamy et al., 2004). The leading edge contains compressed, overlying coronal material and the dark void has a cavity with low density . The core may correspond to an erupting prominence . These features are readily distinguished in white light. The chosen data correspond to a three-parts CME (Kahler, 2006). Data from the Extreme-Ultraviolet Imaging Telescope (EIT) onboard SOHO, (Delaboudinière et al., 1995), were used to investigate the CMEs source regions. EIT has a FOV that covers the solar disk and the corona up to 1.5 $R_\odot$, with a pixel size corresponding to 2.6 arcsec. Images in the line of 195 Å were essential for viewing the source region. EIT has four different filters, He II 304 Å, Fe XII 195 Å Fe IX/X 171 Å and Fe XV, 284 Å. The temperature-sensitive ratio is (Fe XII 195 Å)/(Fe IX/X 171 Å) (Defise et al., 1995).

The Sun–Earth Connection Coronal and Heliospheric Investigation (SECCHI; Howard et al., 2000) instrument suite for the STEREO spacecrafts. The STEREO instrument suite consists of five telescopes covering a broad range of fields of view. The COR1 and COR2 coronagraphs image the inner and outer corona from 1.4 to 15 $R_\odot$. COR1 A, B has a resolution of 7.5 arcsec/pix and field of view (1.4–4 $R_\odot$). COR2 A, B has a resolution

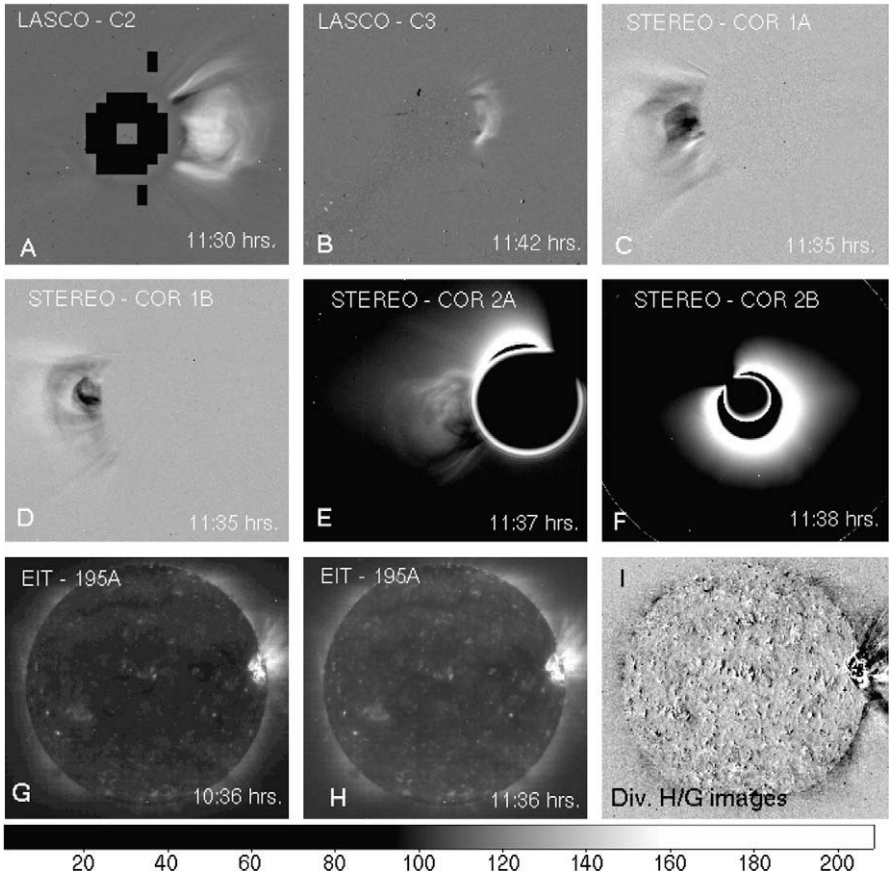

Fig. 1. A CME observed on 2 January 2008 with a characteristic three-part structure is shown at different projection angles as observed with different instruments – (A) LASCO C2, (B) LASCO C3, (C) STEREO COR1A, (D) STEREO COR1B, (E) STEREO COR2A, (F) STEREO COR2B. An active region can be seen at the extreme right of the images (G) and (H) LASCO EIT (with a time difference of 1 h). In panel (I) we show the H/G ratio image to clearly illustrate this active region.

14.7 arcsec/pix and field of view (2–15 $R_{\odot}$). The Heliocentric distances (AU) for STEREO-B, STEREO-A and the Earth were 1.011295, 0.967365 and 0.983281, respectively, at the time of observation (2008/01/02, 11:30 UT).

Fig. 1 shows the images taken on 2 January, 2008 by LASCO with cameras C2, C3, and by STEREO with cameras COR1A, COR1B, COR2A and COR2B, when the CME intensity was at its maximum and EIT observations at 195 Å. The observations with the different instruments basically correspond to the same time with a small time difference of around 12 min.

4. Results

Fig. 1 shows the three parts that are characteristic of some CMEs – frontal structure, cavity and a core – in A, B, C, D and E images.

The three parts are best seen on the LASCO C2 and STEREO COR2A images (Fig. 1A and E), whereas on the LASCO C3 image the frontal structure is seen as an arc (Fig. 1B). In STEREO COR 1A and STEREO COR 1B, we also see the CME with a three part structure (Fig. 1C and D, respectively). From the COR 2A image, it can be seen that the core is formed of several loops and arcades (Fig. 1E). The observations with EIT at 195 Å show the active region associated with the CME. We show the active region (Fig. 1G and H). Panel 1I shows the H/G ratio image to clearly illustrate this active region.

We have performed a wavelet analysis of all these images. The results from this analysis are presented in Figs. 2–7. Fig. 2 shows the active region seen in the SOHO/EIT images at 195 Å. A zoomed image of the active part observed by SOHO EIT is shown in the right panel, where we can see that the active region is characterized by complex structures. In panel A, we show a superposition of EIT and SOHO images, where we can see the relationship between the active region and CME. In panel B, we show the wavelet analysis of this region over a scale of 2 pixels, which shows a very complex structure. Thus, the active region seems to contain the seeds that grow into complex CME structures with expanded loops.

Figs. 3–7 have the following format: the first image on the upper left panel corresponds to the original white light image, followed by images showing structures at chosen wavelet scales of 3, 5 and 7 pixels, respectively, in panels (A), (B) and (C).

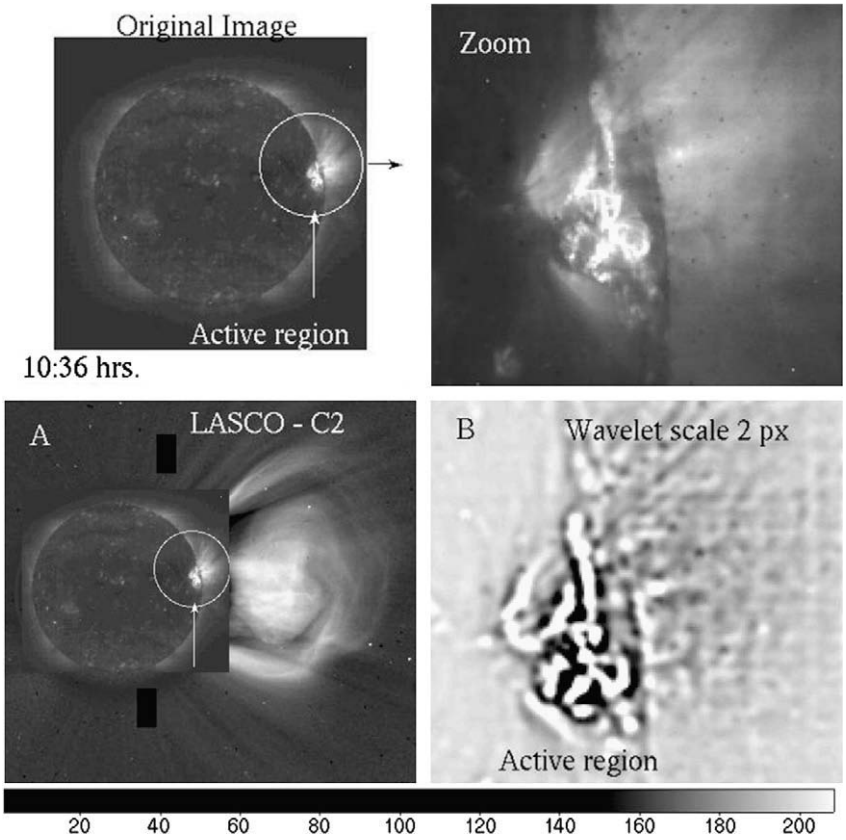

Fig. 2. Wavelet analysis of EIT 195 Å observed on 2 January 2008. We can to see the active region. We show the relationship between CME and the active region.

In the LASCO C2 image (Fig. 3), all of the three parts of the CME can be seen very well (original image). At the 3-pixel scale = 0.035 $R_\odot$ (Fig. 3A), we can see the complex structures in the core that suggest "intertwined" magnetic field lines forming arcs and also jet-like structures defining the boundary of the CME (denoted by letters (**a**, **b**)). Narrow arcs are also seen in the frontal structure forming various circular sectors. In (B) (5 pixels = 0.059 $R_\odot$), the core shows distorted filamentary structures (**a**). Further to the right (in the box), the arcs seen at the 3 pixel scale are also seen in the 5-pixel scale (**b**). The arcs are seen at higher contrast at this scale. In (C) (7 pixels = 0.083 $R_\odot$), we can see all the structures seen in (B). An additional structure can be seen in this image, which is denoted by letter (**c**). From this analysis, we can see that the core has a complex structure, possibly formed by several magnetic arcades where the field appears to be twisted. It can also be seen that the frontal structure is made up of several concentric arcs.

In the LASCO C3 image (Fig. 4), the characteristic three parts of the CMEs are not seen. Instead only the frontal structure is seen as a thick arc in all the plotted scales (3, 5 and 7 pixels corresponding to physical scales of 0.175, 0.292 and 0.409 $R_\odot$, respectively).

The wavelet analysis of the COR 1A image is shown in Fig. 5. At the 3 pixel = 0.023 $R_\odot$ scale (Panel A), we can see the internal structure of the core. It can be noticed that the core is resolved into several radially complex structure, surrounded by arch-shaped structures. Further out extended arcades bound the CME, with several radial structures surrounding it on either side. At higher wavelet scales 5 pixels = 0.039 $R_\odot$, panel B and 7 pixels = 0.054 $R_\odot$, panel C, the external arcades and the flanks become increasingly pronounced. The internal arc to jet contrast is also larger in these higher wavelet scale images. These images suggest that the magnetic configuration inside the core is very different that in the external parts of the CME.

Fig. 5C shows the wavelet analysis (7 pixels = 0.054 $R_\odot$), we observe the same structures as in A and B, there are more flanks in the internal structures clearly and structures are the biggest.

Fig. 6 corresponds to the COR 1B image, which has the same physical scale as that for COR 1A, but seen from another location. We can recover all the structures that are seen in the wavelet analysis of COR 1A. However, the external rainbow of arcades is seen almost projected onto the internal arcs (or core) at this orientation. This illustrates that our analysis is able to pick out the basic internal structures even when seen from two different orientations.

In the COR2A image (Fig. 7), we can see a broad view of the CME. The details of the frontal structure associated with the three-part CME are better seen in this image. In Panel A (3 pixels – 0.046 $R_\odot$), we can see the structure of the core. At the resolution of this instrument the flanks

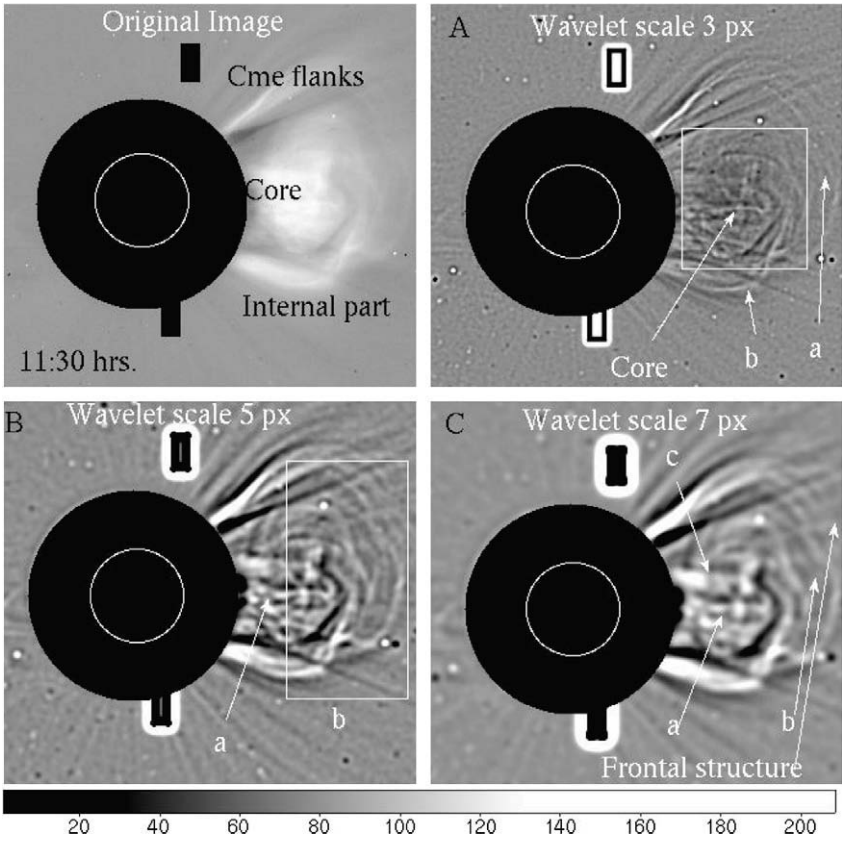

Fig. 3. LASCO C2 image of a three-part CME observed on 2 January 2008. Panels (A–C) show the diferents scales of the analysis wavelet and we show the different structures of the CME found with the wavelet analysis.

seen in the COR1A image are not visible, but the arcs surrounding these flanks are clearly seen. In Fig. 7B (5 pixels = 0.076 $R_\odot$) and C (7 pixels – 0.107 $R_\odot$), the arcs become more prominent – which is very similar result to the analysis of the COR 1A and COR 1B images. Between the internal arc and the external rainbow structure of arcades (frontal structure), several concentric arcs are seen.

5. Orientation of the most intense flux

Another study that was carried out was to measure the direction or angle of a structure immersed in a CME. To do this, we have taken an elliptical diaphragm (with a major axis of 80 pixels and a minor axis of 20) centred on a given pixel of the image, with its major axis at an angle ϕ with respect the x-axis. We have then computed the total flux

$$I_\phi(x,y) = \int\int_{s(\phi,x,y)} I(x',y')dx'dy', \tag{3}$$

within the diaphragm. In this equation, $s(\phi,x,y)$ represents the surface enclosed by the elliptical diaphragm (centred in x,y, and at an angle ϕ). We then associate the direction of the structures at the position of the central pixel with the angle ϕ_m for which we obtain the maximum over all ϕ of $I_\phi(x,y)$. This procedure is repeated with the elliptical diaphragm centred on each pixel of the image.

Through this process, we obtain directions (associated with the values of ϕ_m) which point along the axes of bright, filamentary structures. In regions corresponding to "valleys" limited by two filamentary structures, the directions associated with the values of ϕ_m point towards the neighbouring filaments, bridging the bottom of the valley.

Then, for each pixel (x,y) of the image, we obtain a "preferred orientation" $\phi_m(x,y)$, which we plot as lines of equal moduli at the corresponding positions and orientations. These "arrow plots" are shown in Fig. 8. The arrows in this figure show the orientation of the emitting structures. The results are illustrated for the images from LASCO C2 and STEREO COR 2A (see Figs. 8 and 9), in which all three parts of the CMEs are seen.

The arcs and flanks associated with the CME that are seen with the wavelet analysis can also be seen in these two vector diagrams.

6. Discussion and conclusions

It can be seen that the loop structures inside a CME are better defined in the processed wavelet images than in the original images. At small scales (3 and 5 pixels), the core is the only part that is seen, while the bright edge is the dominant structure at large scales (7 pixels), and traces an almost circular loop. On closer examination, we can

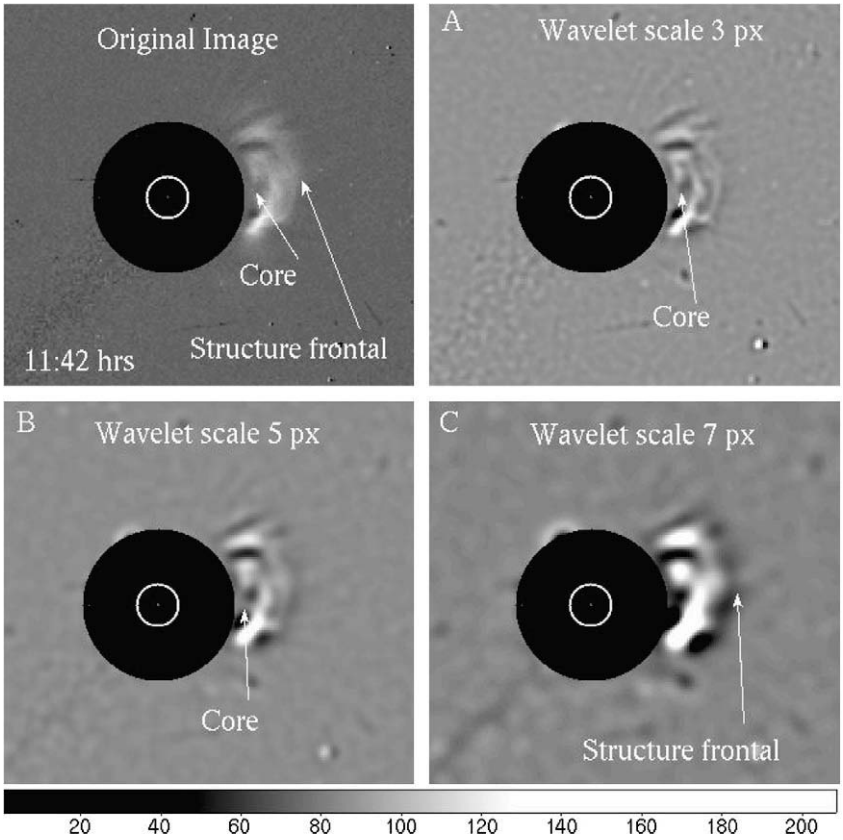

Fig. 4. LASCO C3 image of CME observed on 2 January 2008, only the leading edge is seen as a thick arc in all the plotted scales (3, 5 and 7 pixels).The bright ring inside the dark disk indicates the location and diameter of the Sun. The outer edge of the disk lies at ~3.5 solar radii.

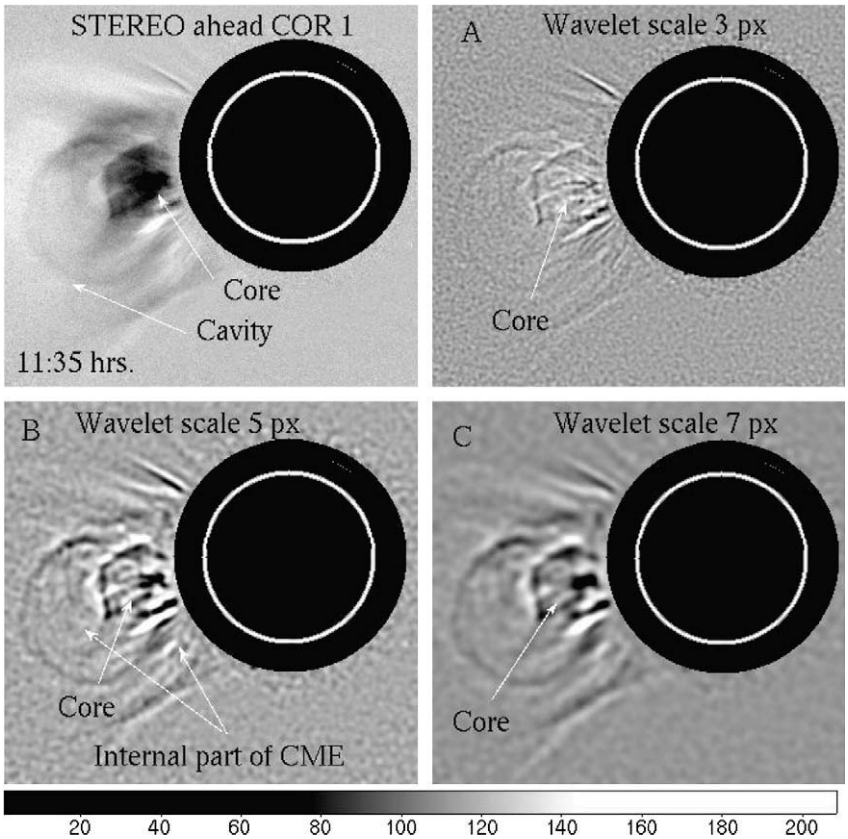

Fig. 5. COR 1A image of the CME shows in Fig. 1. Panels (A–C) show the results from wavelet analysis at three selected scales.

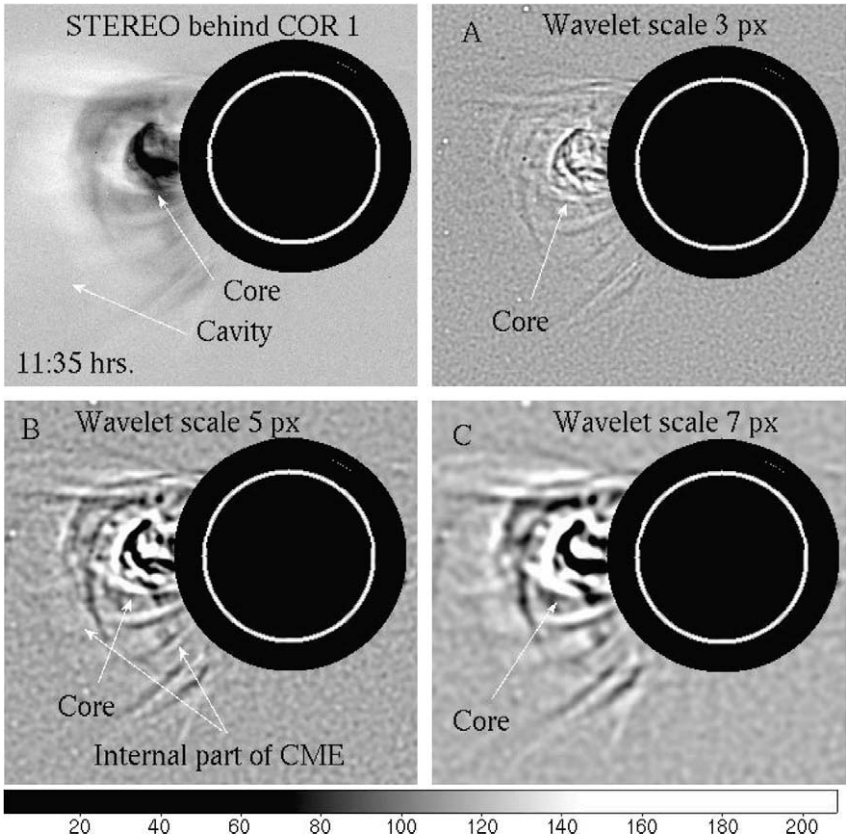

Fig. 6. The same as in Fig. 5, but for the COR 1B image.

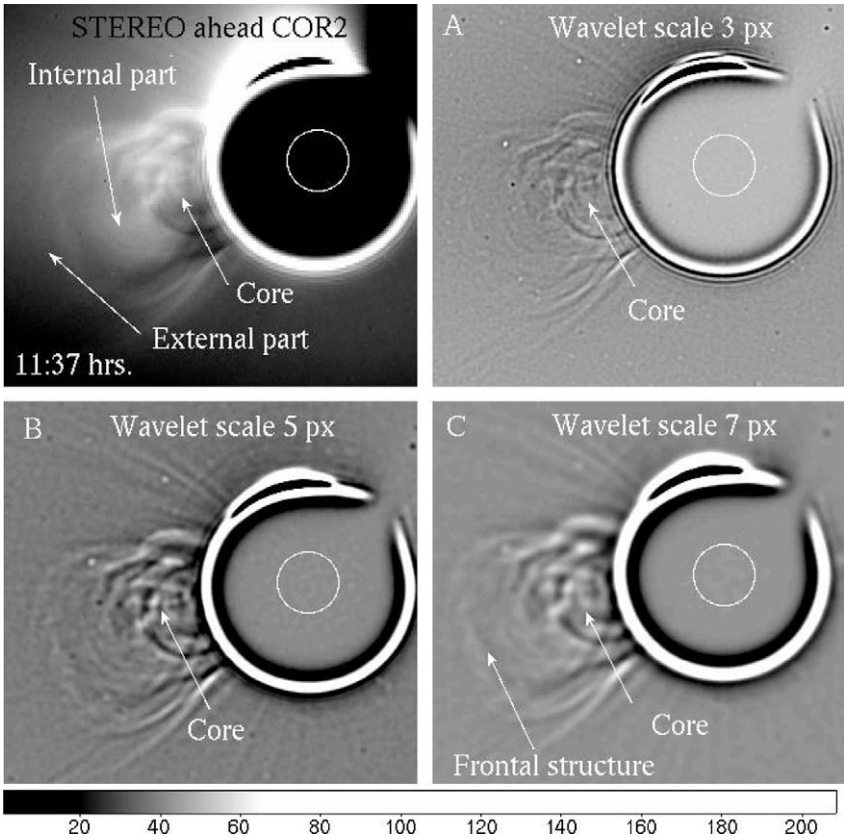

Fig. 7. Results of wavelet analysis of COR 2A image. We can see a series of arcs one behind the other emanating from the core of the CME in all scales (3, 5 and 7 pixels).

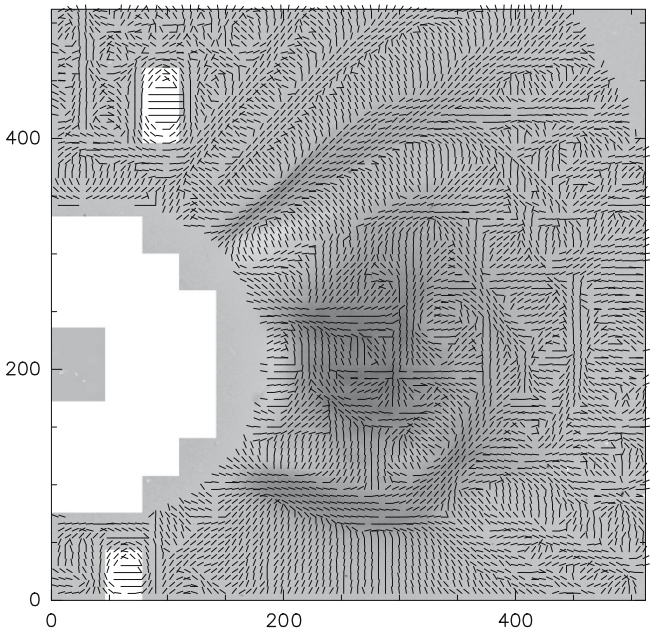

Fig. 8. Vectors showing the orientation of the most intense parts of the structures seen in a CME. The analysis is done only for the part of the original image centered on the CME.

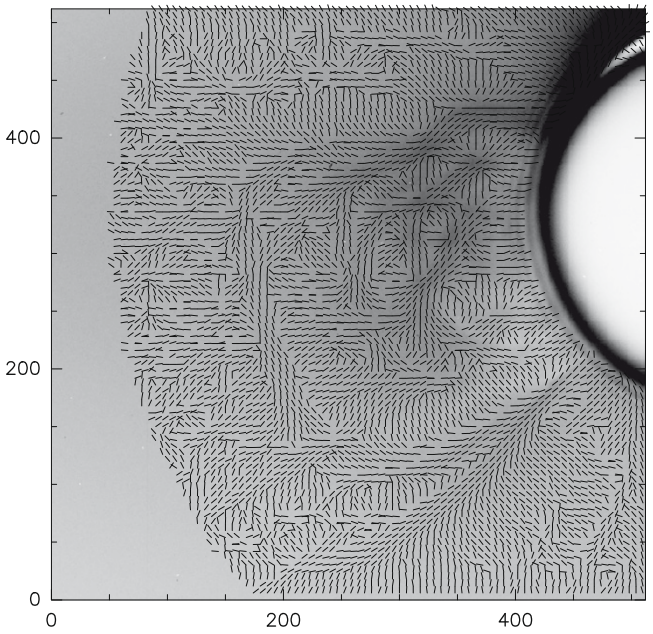

Fig. 9. The same as in Fig. 9, but for the COR 2A image.

see intertwined loop sub-structures inside the core. Also, the circular loop seems to be located in a plane behind the core. The circular pattern or twisted observed within the cavity of the CME suggests the existence of helical magnetic features (Chen et al., 1997; Dere et al., 1999; Wood et al., 1999), commonly known as flux ropes, and used extensively by CME modelers.

In the three-part CME studied in this work, substructures can be clearly seen in the core and in the frontal structure. The core is formed by several radially complex structure surrounded by an arc, whereas the frontal structure is split into a series of concentric rainbow-like arcades. The observed structure of the CME confirms that coronal loops are often reconfiguring via reconnection, and suggests that the core magnetic structures are twisted and more complex than in the outer part of the CME. In the ultraviolet image of the active region, we find many complex sub-structures, similar to those found in the CME.

In Figs. 3–7, we have demonstrated that we can recover the three-part structure of the CME irrespective of the image used to analyze it. However, different instruments have different image scales, which should be taken into account in comparing these images.

The availability of images of the same CME event observed by different cameras in different satellites has allowed us to carry out a study to compare and differentiate the structures of the CME as seen from different angles and with different scales. Using the wavelet analysis technique, we have illustrated that different sub-structures of the CME stand out at different scales. Wavelet decomposed images taken with different cameras look very similar when they are matched to the same physical scale.

Our study has shown that the bright leading edge of a CME is constituted of a series of loops, one behind the other. The core is also resolved into intertwined filamentary structures.

To summarize, the present study is an illustration of the results that can be obtained from wavelet analyses of satellite images of CMEs. This is a first step in understanding the results from such analyses, leading towards the development of more quantitative evaluations of the morphology of CMEs based on their spectral characteristics. The eventual aim of these studies would be to be able to classify the observed CME images based on a wavelet analysis of the observed images. This would provide a quantitative method for classifying images of CMEs.

However, one should keep in mind the limitations of such a classification. While a wavelet analysis method can in principle provide a quantitative evaluation of the spatial characteristics of the structures seen in an image (e. g., by studying the fluxes at given positions obtained for different a scales), this kind of method will only provide a purely morphological description of CMEs. A more realistic, physical classification of course will depend on future studies of the physical properties (e. g., density, temperature, flow velocity) of the ejected material.

References

Bemporat, A., Raymond, J., Poletto, G., Romoli, M. A comprehensive study of the initiation and early evolution of a coronal mass ejection from ultraviolet and white-light data. Apj 655, 576–590, 2007.

Brueckner, G.E., Howard, R.A., Koomen, M.J., et al. The Large Angle Spectroscopic Coronagraph (LASCO). SoPh 162, 357–402, 1995.

Byrne, J.P., Gallagher, P.T., McAteer, R.T.J., Young, C.A. The kinematics of coronal mass ejections using multiscale methods. A&A 495, 325–334, 2009.

Chen, J., Howard, R. A., Brueckner, G. E., et al. Evidence of an erupting magnetic flux rope: LASCO coronal mass ejection of 1997 April 13. ApJ 490, L191, 1997.

Cremades, H., Bothmer, V. On the three-dimensional configuration of coronal mass ejections. A&A 422, 307–322, 2004.

Defise, J.-M., Song, X.Y., Delaboudiniere, J.P., et al. Calibration of the EIT instrument for the SOHO mission, in: Proc. SPIE, vol. 2517, p. 29–39, 1995.

Delaboudinière, J.-P., Artzner, G.E., Brunaud, J., et al. EIT: Extreme-ultraviolet imaging telescope for the SOHO mission. SoPh 162, 291–312, 1995.

Dere, K.P., Brueckner, G.E., Howard, R.A., Michels, D.J., Delaboudiniere, J.P. LASCO and EIT observations of helical structure in coronal mass ejections. ApJ 516, 465–474, 1999.

Fleck, B., Domingo, V., Poland, A.I. The SOHO mission. SoPh 162 (1–2), XII + 531 p, 1995.

Gopalswamy, N., Lara, A., Yashiro, S., Nunes, S., Howard, R.A. Coronal mass ejection activity during solar cycle. ESASP 23, 403–414, 2003.

Gopalswamy, N., Yashiro, S., Vourlidas, A., Lara, A., Stenborg, G., Kaiser, M.L., Howard, R.A. Coronal mass ejections when the Sun went wild. AAS, 204G–4709G, 2004.

Gosling, J.T. Physical nature of the low-speed solar wind. AIPC 17–385G, 1997.

Howard, R.A., Sheeley Jr., N.R., Michels, D.J., Koomen, M.J. Coronal mass ejections – 1979–1981. JGR 90, 8173–8191, 1985.

Howard, R.A., Moses, D.J., Socker, D.G. Sun–Earth connection coronal and heliospheric investigation (SECCHI), in: Proc. of SPIE, vol. 4139, pp. 259–283, 2000.

Hundhausen, A.J. Coronal mass ejections. Cosmic winds and the heliosphere. AASP, 259, 1997.

Hundhausen, A. Coronal mass ejections, in: Strong, K.T., Saba, J.L.R., Haisch, B.M., Schmelz, J.T. (Eds.), The Many Faces of the Sun: A Summary of the Results from NASA's Solar Maximum Mission. Springer, New York, p. 143, 1999.

Illing, R.M.E., Hundhausen, A.J. Possible observation of a disconnected magnetic structure in a coronal transient. JGR, 8810210I, 1983.

Kahler, S.W. Solar flares and coronal mass ejections. ARA&A, 30K–113K, 1992.

Kahler, S.W. Observational properties of coronal mass ejections. GMS, 21–32, 2006.

MacQueen, R.M., Eddy, J.A., Gosling, J.T., et al. The outer solar corona as observed from Skylab: preliminary results. JAp 187, L85–L88, 1974.

Stenborg, G., Cobelli, P.J. A wavelet packets equalization technique to reveal the multiple spatial-scale nature of coronal structures. A&A 398, 1185–1193, 2003.

Stenborg, G., Vourlidas, A., Howard, R.A. A fresh view of the extreme-ultraviolet corona from the application of a new image-processing technique. Apj 674, 1201–1206, 2008.

Tousey, R. The Solar Corona, in: Rycroft, M.J., Runcorn, S.K. (Eds.), Space Research XIII. Akademie, Berlin, pp. 713–713, 1971.

Webb, D.F., Jackson, B.V., Reames, D.V. Study of CMES observed in the heliosphere using HELIOS photometer. Magnetic field and plasma data. BAAS, 24W–747W, 1992.

Wood, B.E., Karovska, M., Chen, J., Brueckner, G.E., Cook, J.W., Howard, R.A. Comparison of two coronal mass ejections observed by EIT and LASCO with a model of an erupting magnetic flux rope. ApJ 512, 484–495, 1999.

Yashiro, S., Gopalswamy, N., Michalek, G., et al. A catalog of white light coronal mass ejections observed by the SOHO spacecraft. JGRA, 10907105Y, 2004.